Analysis of angular-selective performances of obliquely deposited birefringent thin film

Yongqiang Hou (侯永强)[1,2], Hongji Qi (齐红基)[1*], Kui Yi (易 葵)[1], and Jianda Shao (邵建达)[1]

[1] *Key Laboratory of Materials for High Power Laser, Shanghai Institute of Optics and Fine Mechanics, Chinese Academy of Sciences, Shanghai 201800, China*

[2] *University of Chinese Academy of Sciences, Beijing 100049, China*

[*] *Corresponding author: qhj@mail.siom.ac.cn*

Received May 26, 2013; accepted September 4, 2013; posted online September 29, 2013

A slanted columnar TiO_2 sculptured anisotropic thin film is prepared using the glancing angle deposition (GLAD) technique. We extend the inference regarding the optical properties of a uniaxial birefringent film based on theoretical analysis to include the more general case of a multilayer biaxial birefringent thin film, the optic axis of which is in the incident plane. We also investigate in detail the symmetrical angular-selective transmittance performances of TiO_2 biaxial anisotropic thin films for light incident at the same angle but coming from opposite sides of the surface normal. The tilted nanocolumn microstructures of the birefringent thin films induce optical anisotropy. The transmisson spectra for the *p*-polarized wave of TiO_2 biaxial anisotropic thin film measured in the experiment almost overlap at the symmetrical oblique incidence at the $\pm\theta_0$ angles, which validates our theoretical derivation.

OCIS codes: 310.6860, 260.1440, 230.4000.

doi: 10.3788/COL201311.103101.

Crystal birefringence is derived from the anisotropy of crystalline molecules and their unit cells. The anisotropic microstructures of thin films also induce optical anisotropy, which are called sculptured thin films (STFs)[1]. Since the emergence of obliquely deposited thin films, three dimensional (3D) nanoengineered anisotropic STFs prepared using the GLAD technique and resembling artificial materials with interesting optical properties have been extensively adopted in the design and development of optical polarizing components, including phase-retardation devices[2], polarization-selective beam splitters[3], polarizers[4] and polarization converters[5], broadband antireflective coatings[6] and rugate filters[7]. In contrast to conventional optical components that are constructed from isotropic thin films, these devices perform better in terms of manipulating the polarization states of electromagnetic waves because the STF presents birefringence. The nanostructures of GLAD films range from simple microstructures, e.g., oblique column, zigzag, and helix[8], to exotic nanostructures such as polygonal spirals[9] with state-of-the-art technology. Meanwhile, the development of the substrate sweep[10] and bideposition technique[11] enables flexible coating designs, thus easily obtaining stable nanostructures of GLAD thin films. In addition, these films are deposited in a controllable manner during the growth process; thus, the nanocolumn microstructures exhibit continuum and anisotropic characteristics but the small-sized molecules and clusters retain their individuality. The densities of these films are significantly lower than those of their bulk counterparts as a result of the self-shadowing effects and limited surface diffusion mobility of obliquely deposited atoms. As a consequence, the STFs also meet the requirements of a variety of technical applications, such as catalytic surfaces[12], micro-sensor elements[13] and 3D photonic crystals[14] by virtue of their high porosity, periodicity, and chirality. These properties are very important for the development of integrated optical system miniaturization.

Prior to the preparation of the anisotropic thin-film device, characterizing the optical properties of the sculptured birefringent thin film, including its symmetrical angular-selective performances, is more important. When the optic axis of a uniaxial crystal is not parallel or perpendicular to the crystal interface, the propagating behaviors of the extraordinary wave are completely different for light that is symmetrically incident at the same angle but coming from opposite sides of the surface normal, although the principal section coincides with the principal plane. However, the interference effects between the interfaces of the uniaxial birefringent thin-film layers should be considered when the wave is propagated across and through the thin film as a result of the multiple reflections on the film substrate interface. As a result, the propagating properties of the electromagnetic waves generally differ from those in the uniaxial crystal. To date, theoretical analysis and experimental study of angular-selective performances of birefringent thin films have achieved a great deal of progress. However, this research is mainly focused on metal layers or metal–dielectric films. The transmittances of the metal layer vary, and significant angular-selective performances are shown, which are attributed to the improved absorption of the metal layer when light is symmetrically incident with the $\pm\theta_0$ angles[15]. In this letter, we firstly extend the theoretical analysis results derived from the case of a uniaxial birefringent thin film to the more general case of a multilayer biaxial birefringent thin film. We then experimentally investigated the angular-selective transmittance performances of a biaxial birefringent thin film to verify the validity and generality of our theoretical derivation. TiO_2 has been selected as the

material for oblique deposition because of its high bulk refractive index, good mechanical and thermal stability, high static dielectric constant, and excellent transparency at visible wavelengths. Moreover, the low-dimensional structures of TiO_2 have a huge potential as a result of their photoinduced and nonlinear optical properties[16] and are promising photovoltaic cell materials[17]. The large specific surface area of the obliquely deposited thin films is also suitable for photocatalysis application[18−21]. In addition, the optical properties of TiO_2 do not change significantly over common environment ranges.

In general, the coupling of two orthogonal polarized waves makes dealing with the electromagnetic propagation in a birefringent thin film difficult. When the principal section of a uniaxial birefringent thin film (n_o,n_o,n_e) is consistent with the principal plane, that is, the optic axis lies in the plane of incidence, the *s*- and *p*-polarized waves decouple. In this case, the transverse electric (TE)wave propagates in an ordinary manner and is independent of the propagation direction. The optical properties of the birefringent thin film are equivalent to those of the isotropic thin film with the same thickness. Therefore, we do not discuss the *s*-polarized wave in this work. By contrast, the transverse magnetic (TM) wave propagates in an extraordinary manner, and the propagating directions of the wave vectors are not generally similar to those of rays within the birefringent thin film. Under the standard boundary continuity conditions of Maxwell's equations, our previous study[22−24] has deduced the resultant electric- and magnetic-field vectors of the extraordinary wave at the interfaces. Our previous study also deduced the propagating parameters in a uniaxial birefringent thin film, such as the forward- and backward-propagating directions of the wave vectors, rays, and their corresponding refractive indices. The 2×2 characteristic matrix, including the multiple reflections for the extraordinary wave, is derived and represented below

$$\frac{1}{\eta_+ + \eta_-}\begin{bmatrix} \eta_- e^{i\delta_+} + \eta_+ e^{-i\delta_-} & e^{i\delta_+} - e^{-i\delta_-} \\ \eta_-\eta_+(e^{i\delta_+} - e^{-i\delta_-}) & \eta_+ e^{i\delta_+} + \eta_- e^{-i\delta_-} \end{bmatrix}, \tag{1}$$

where $\delta_+ = \frac{2\pi}{\lambda} n(\alpha_1) d\cos\theta_1$ and $\delta_- = \frac{2\pi}{\lambda} n(\alpha_2) d\cos\theta_2$ denote the phase thicknesses of the forward- and backward-traveling extraordinary waves, respectively. The effective optical admittances determined by the propagating directions of wave vectors and the corresponding refraction indices are given as $\eta_+ = \frac{n(\alpha_1)}{\cos\theta_1}$ and $\eta_- = \frac{n(\alpha_2)}{\cos\theta_2}$, respectively.

With the characteristic matrix given above, we can derive the input optical admittance $Y = \frac{C}{B}$, the reflectance R, and the transmittance T of the birefringent thin film for light incident at an arbitrary incidence angle θ_0, as with an isotropic dielectric thin film, as follows[25]:

$$R = \left(\frac{\eta_0 B - C}{\eta_0 B + C}\right)\left(\frac{\eta_0 B - C}{\eta_0 B + C}\right)^*, \tag{2}$$

$$T = \frac{4\eta_0\eta_g}{(\eta_0 B + C)(\eta_0 B + C)^*}. \tag{3}$$

B and C are the normalized electric and magnetic fields at the front interface and can be used to extract the optical properties of the birefringent thin film. $\eta_0 = n_0/\cos\theta_0$ and $\eta_g = n_g/\cos\theta_g$ represent the effective optical admittance of the incident medium and the substrate for the $p-$polarized wave, respectively.

On the basis of the theoretical derivation above, we then experimentally discuss the angular-selective performances of the extraordinary wave incident at the same angle but coming from opposite sides of the surface normal in detail. The slanted columnar TiO_2 birefringent thin film was deposited onto flat fused silica (Φ30× 3 (mm)) substrate using reactive-electron beam evaporation in a laboratory high-vacuum deposition system configured for the GLAD technique. This method utilizes physical vapor deposition to deposit films on a substrate that is tilted at a deposition angle toward the vapor source, as shown schematically in Fig. 1. The tilting and rotating of the substrate were automatically controlled by two step motors. Therefore, the void region between the nanocolumns and the volume fraction of the deposited STF can also be controlled using this process. An INFICON IC/5 quartz crystal monitor was located near the substrate and used to measure the deposition rate and thickness of the growing film. A well-controlled deposition rate resulted in a uniform pitch. In our experiment, the substrate was ultrasonically cleaned in acetone and ethanol before being introduced into the vacuum system. The deposition angle α, which was measured as the impinging direction of the incident vapor flux with respect to the substrate normal, was fixed at 70°. During the deposition process, the substrate was maintained at room temperature without rotation. The chamber base pressure was pumped to less than 2.0×10^{-3} Pa. To maintain the stoichiometry of the TiO_2 birefringent thin film, ultrahigh-purity O_2 (99.99%) was incorporated to obtain a background pressure of 2.7×10^{-2} Pa during the growth of the thin film. As the sample was being prepared, thermal annealing at 773 K was carried out for 4 h in the muffle furnace atmosphere.

With regard to the tilted nanocolumnar film deposited using the GLAD technique, the anisotropic microstructures of the birefringent thin film are generally biaxial,

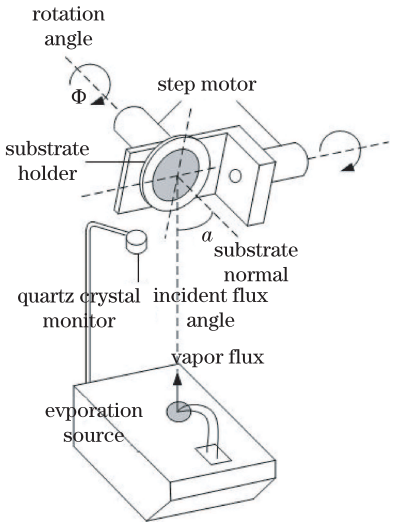

Fig. 1. Schematic of the GLAD process.

where one of the principal axes (labeled 1) is oriented in the direction of the columns. The other principal axis (labeled 2) is perpendicular to the direction of the columns and located in the deposition plane. The third principal axis (labeled 3) is perpendicular to the incidence plane, as shown in Fig. 2. The incident medium and substrate are homogeneous and isotropic media. Thus, the optical properties of the biaxial birefringent thin film are determined by the three principal refractive indices n_1, n_2, n_3, coating thickness d, and column angle Ψ. In the y–z incident plane, the biaxial thin film degenerates to a uniaxial thin film, with the inclined optic axis denoted by column angle Ψ because of the decoupling of the TE and TM waves. In this case, the s-polarized wave propagates in an ordinary manner with the index of refraction n_3 and is irrelevant to the optical properties of a TM wave. A TM wave is extraordinary because the electromagnetic propagating behavior is dependent on the principal refractive indices n_1, n_2, and column angle Ψ. As a consequence, the optical constants of the biaxial birefringent thin film for s- and p-polarized waves can be determined from the transmission spectra using the characteristic matrix above[26].

The morphology of the birefringent thin film was observed by field emission scanning electron microscopy (FE-SEM)(S-4700, Hitachi, Japan). For improved SEM observation, the TiO_2 anisotropic thin film deposited on n-Si(100) substrate was cleaved down the deposition plane and coated with a thin layer of gold to improve conductivity. To investigate the angular-selective performances of the biaxial birefringent thin film, the transmission spectra $T_{s,p}(\lambda, \theta_0)$ were obtained by a spectrophotometry (UV/VIS/NIR Lambda 1050, Perkin-Elmer, USA)in air from 400 to 850 nm with various symmetrical incidence angles. The spectral resolution and wavelength accuracy were less than 0.05 nm and ±0.08 nm at the UV/VIS region and less than 0.20 nm and ±0.30 nm at the NIR region, respectively. The schematic diagram of the measurement device is shown in Fig. 3. The polarizer was introduced into the light path to obtain two orthogonal polarization waves. In our measurements, an integrated sphere was used in the detector and a blank fused silica substrate was inserted between the sample and the detector to eliminate the beam shift effect at the oblique incidence. The position of the sample was carefully adjusted when measured at different incidence angles; thus, the incident plane coincides with the deposition plane, which is defined as the direction of column growth with respect to the substrate normal. The transmittance T_f of the thin film without the back reflection of the substrate can be obtained according to the formula $T_f = (1 - R_G)/(T_G/T - R_G)$, where T, T_G, and R_G represent the raw transmittance of the sample, the transmittance of the air–substrate interface, and the reflectance of air–substrate interface, respectively.

The SEM images of the TiO_2 birefringent thin film are shown in Fig. 4. As shown in the top-view and cross-sectional morphologies, the film grew with a loose and porous columnar structure that was slanted toward the vapor flux, owing to the self-shadowing and surface diffusion effects. Pores among the nanocolumns are a significant characteristic of GLAD- produced films, and the porous structure inevitably influences the optical

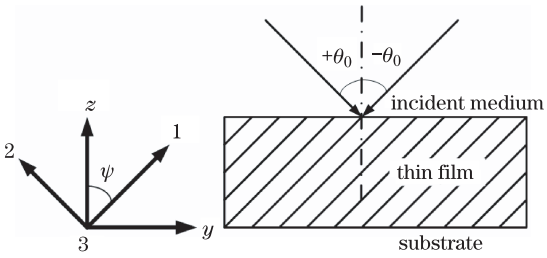

Fig. 2. Schematic of a biaxial birefringent thin film model.

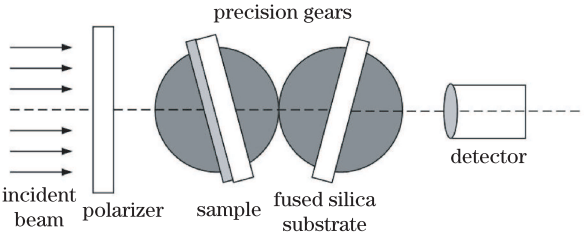

Fig. 3. Schematic of the polarization transmittance measurement device.

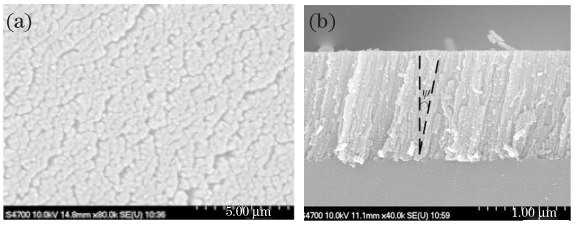

Fig. 4. Top-view (a) and cross-sectional (b) SEM images of the TiO_2 birefringent thin film deposited at $\alpha = 70°$.

performances of the birefringent thin film. The typical sculptured microstructures with highly orientated tilted nanocolumns are exhibited in Fig. 4(b). The thickness and oblique angle of the nanocolumns were measured to be approximately 1200 nm and 12°, respectively. Optical anisotropic permittivity tended to occur in thin films consisting of these columns, which is attributed to the anisotropic distribution of nanocolumns.

The transmission spectra of the TiO_2 birefringent thin film measured at the symmetrical oblique incidences of ±20°, ±30°, ±45°, and ±60° for the TM wave are plotted in Fig. 5(a). The transmission measurements of two polarized waves at normal incidence are also shown in Fig. 5(b) for improved comparison. As shown in Fig. 5, the transmittance spectra appeared as obvious interference modulations as a result of the multiple reflections at film interfaces. The spectra separated at normal incidence for both TE and TM waves, indicating that our prepared TiO_2 sculptured birefringent thin film consisting of highly orientated microstructures composed of slanted nanocolumns was optically anisotropic. In addition, the anisotropic thin film was highly transparent above 600 nm at normal and oblique incidence, whereas a strong absorption in the UV band was observed. This behavior is common in TiO_2 birefringent thin films annealed at elevated temperatures and is generally attributed to the scattering caused by grain coarsening, densification, and rearrangement of the columnar microstructures as a result of increasing surface roughness. Meanwhile, the

improved absorption as a result of oxygen vacancies also decreased the transmittance[27]. Furthermore, as the incidence angle increased, the spectral performance shifted toward shorter wavelengths (blue-shift), and the peak-valley (PV) values of interference fringes attenuated for the TM wave. When the incidence angle increased to $\pm 60°$, the interference effects became weaker and the PV values were almost zero. This phenomenon is known as the Brewster effect.

The optical constants for the TiO_2 birefringent thin film were derived on the basis of the biaxial birefringent thin film model and Cauchy dispersion equations by fitting the transmission spectra for *s*- and *p*-polarized waves with an inverse synthesis method. The initial values of dispersion coefficients were gradually adjusted until improved optimization of the experimental measurements and theoretical calculations was achieved. The dispersion of the three principle refractive indices and extinction coefficients are exhibited in Figs. 6(a) and (b). Meanwhile, the optimization also provided a coating thickness $d = 1238.949$ nm and a column angle $\Psi = 12.179°$, which agreed reasonably well with the SEM image. By employing the extracted structural parameters, the transmittance fitting curves for two polarized waves were inversely calculated. The results are shown in Figs. 5(a) and (b). The theoretical fitting curves clearly coincided with the experimental measured spectra, thereby validating the model established for this kind of GLAD-produced film, as well as the improved generality and superiority of the characteristic matrix. In particular, the measured transmission spectra of the TiO_2 birefringent thin film for the TM wave almost overlapped at the symmetrical oblique incident with the $\pm\theta_0$ angles, as shown in Fig. 5(a). This result is consistent with our theoretically predicted results, which validates our derivation. Slight deviations and drifts in the transmittances measured at the symmetrical oblique incidence angles $\pm\theta_0$ are mainly attributed to the

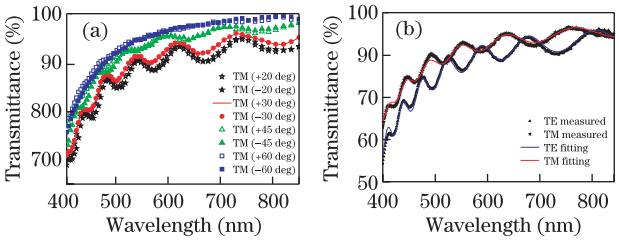

Fig. 5. Transmission spectra of the TiO_2 birefringent thin film measured as-deposited at symmetrical oblique (a) and normal incidence (b).

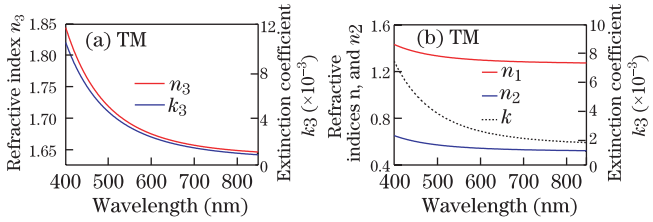

Fig. 6. Dispersion of the principle refractive indices and extinction coefficients as determined by the transmission spectra of TiO_2 birefringent thin film for (a) TE and (b) TM waves.

anisotropic scattering and adsorption caused by the idealized optical model, as well as nanostructure confinement effects and inherently large surface-to-volume ratio. Moreover, the non-uniformity of our prepared tilted columnar birefringent thin film, which is induced by the self-shadowing effect and limited mobility of the deposited atoms, may have a role in the optical properties of film interfaces and may form some space non-uniform distribution of the refractive indices. The spectral performance changes produced by non-uniformity are very sensitive to the incidence angle, wavelength, and polarization[28]. In addition, the porous property of the obliquely deposited thin film also contributes to the diffusion scattering effects and the decrease in transmittance because of the large number of air/film interfaces within the thin film microstructures. In this case, each interface acts as a discontinuity in the refractive index. With the increase in the refractive index, the scattering strength of the interfaces is enhanced accordingly. Finally, TiO_2 has demonstrated the photocatalytic self-cleaning phenomenon, where the ultraviolet illumination of TiO_2 generates electron-hole pairs that react with organic contaminants on the surface to produce several compounds, including CO_2 and H_2O, which desorb from the surface[29,30]. This self-cleaning effect reduces the aging of the birefringent thin film and may have an effect on angular-selective performances. The effects of anisotropic scattering and adsorption and the non-uniformity of the birefringent thin film on the angular-selective performances must be investigated and quantified in a controlled environment in further research.

In conclusion, we firstly extend the inference regarding the optical properties of a uniaxial birefringent thin film based on theoretical analysis to the more general case of a multilayer biaxial birefringent thin film, the optic axis of which is in the incident plane. We then investigate the angular-selective transmittance performances of light that is symmetrically incident at the same angle but coming from opposite sides of the surface normal. To verify the validity and generality of our theoretical derivation, a slanted columnar TiO_2 biaxial anisotropic thin film is prepared via the GLAD technique using reactive-electron beam evaporation. The morphology of the TiO_2 birefringent thin film is examined using SEM, and the transmission spectra are obtained by spectrophotometry with various symmetrical incidence angles. The results show that the tilted nanocolumn microstructures of the birefringent thin film induce optical anisotropy. The transmission spectra of the TiO_2 birefringent thin film for the TM wave, which is measured in the experiment, almost overlaps at the symmetrical oblique incident with the $\pm\theta_0$ angles. This result validates our theoretical derivation regarding the angular-selective performances of the biaxial birefringent GLAD-produced film, as well as the improved generality and superiority of the characteristic matrix.

This work was supported by the National Natural Science Foundation of China under Grant No. 61205211.

References

1. K. Robbie, M. J. Brett, and A. Lakhtakia, Nature **384,** 616 (1996).

2. T. Motohiro and Y. Taga, Appl. Opt. **28,** 2466 (1989).
3. H. Qi, R. Hong, K. Yi, J. Shao, and Z. Fan, Appl. Opt. **44,** 2343 (2005).
4. X. Fu, K. Yi, J. Shao, and Z. Fan, Chin. Opt. Lett. **6,** 544 (2008).
5. C. Lin and Y. Jen, J. Nanophotonics **6,** 061507 (2012).
6. J. Xi, M. F. Schubert, J. K. Kim, E. F. Schubert, M. Chen, S. Lin, W. Liu, and J. A. Smart, Nat. Photon. **1,** 176 (2007).
7. J. Zhang, M. Fang, Y. Shao, Y. Jin, and H. He, Chin. Phys. B **21,** 054219 (2012).
8. R. Messier, T. Gehrke, C. Frankel, V. C. Venugopal, W. Otano, and A. Lahktakia, J. Vac. Sci. Technol. **15,** 2148 (1997).
9. A. C. van Popta, M. J. Brett, and J. C. Sit, J. Appl. Phys. **98,** 083517 (2005).
10. Y. Jen, C. Peng, and H. Chang, Opt. Express **15,** 4445 (2007).
11. I. Hodgkinson, Q. Wu, L. De Silva, and M. Arnold, Opt. Express **12,** 3840 (2004).
12. J. G. Gibbs and Y. Zhao, Small **5,** 2304 (2009).
13. Y. Liu, J. Shi, F. Zhang, H. Liang, J. Xu, A. Lakhtakia, S. J. Fonash, and T. Huang, Sensor. Actuat. B-Chem. **156,** 593 (2011).
14. V. C. Venugopal, Proc. SPIE **8465,** 84650V (2012).
15. G. W. Mbise, G. A. Niklasson, C. G. Granqvist, and S. Palmer, J. Appl. Phys. **80,** 5361 (1996).
16. Y. Djaoued, K. Ozga, A. Wojciechowski, A. H. Reshak, J. Robichaud, and I. V. Kityk, J. Alloy. Compd. **508,** 599 (2010).
17. E. Gondek, Y. Djaoued, J. Robichaud, P. Karasinski, I. V. Kityk, A. Danel, and K. J. Plucinski, J. Mater. Sci.-Mater. EL. **23,** 2057 (2012).
18. B. O'Regan and M. Grätzel, Nature **353,** 737 (1991).
19. M. Suzuki, T. Ito, and Y. Taga, Appl. Phys. Lett. **78,** 3968 (2001).
20. J. Yu, M. Zhou, B. Cheng, H. Yu, and X. Zhao, J. Mol. Catal. A-Chem. **227,** 75 (2005).
21. G. K. Kiema, M. J. Colgan, and M. J. Brett, Sol. Energ. Mat. Sol. C **85,** 321 (2005).
22. H. Qi, D. Zhang, J. Shao, and Z. Fan, Europhys. Lett. **70,** 257 (2005).
23. H. Qi, J. Shao, and Z. Fan, Europhys. Lett. **78,** 17004 (2007).
24. Y. Hou, X. Li, K. He, H. Qi, K. Yi, and J. Shao, Chin. Phys. Lett. **30,** 017802 (2013).
25. H. A. Macleod, *Thin-Film Optical Filters* (CRC, Boca Rotan, 2010).
26. H. Qi, X. Xiao, H. He, K. Yi, and Z. Fan, Appl. Opt. **48,** 127 (2009).
27. G. Tian, L. Dong, C. Wei, J. Huang, H. He, and J. Shao, Opt. Mater. **28,** 1058 (2006).
28. H. Qi, M. Zhu, W. Zhang, K. Yi, H. He, and J. Shao, Chin. Opt. Lett. **10,** 013104 (2012).
29. M. T. Taschuk, J. J. Steele, A. C. Van Popta, and M. J. Brett, Sensor. Actuat. B- Chem. **134,** 666 (2008).
30. M. R. Hoffmann, S. T. Martin, W. Y. Choi, and D. W. Bahnemann, Chem. Rev. **95,** 69 (1995).